SLAC-PUB-8409
March 2000

Pulsed RF Breakdown Studies

L. Laurent[a,b], G. Caryotakis[a], G. Scheitrum[a],
D. Sprehn[a], N.C. Luhmann, Jr.[b]

[a]Stanford Linear Accelerator Center, Menlo Park, CA 94025
[b]University of California Davis, Davis, CA 95616

Presented at SPIE Microwave Intense Pulses VII
Orlando, Floria
April 24-26, 2000

*Work supported by Department of Energy contract DE-AC03-76SF00515 and AFOSR under Grant F49620-95-1-0253 (MURI).

Pulsed rf breakdown studies

L. Laurent[a,b], G. Caryotakis[a], G. Scheitrum[a], D. Sprehn[a],
N.C. Luhmann, Jr.[b]

[a]Stanford Linear Accelerator Center, Menlo Park, CA 94025

[b]University of California Davis, Davis, CA 95616

ABSTRACT

A series of experiments have been conducted to investigate the critical mechanisms involved in pulsed rf breakdown. This research has examined fundamental issues such as microparticle contamination, grain boundaries, residual gas, pulse duration, field emission, and the spatial distribution of plasma during a breakdown event. The motivation of this research is to gain a clearer understanding of the processes involved in breakdown and to determine methods to increase the breakdown threshold thereby increasing the available power in high power microwave sources and accelerator components.

Keywords: Breakdown, field emission, grain boundaries, x-rays, microparticles, surface plasma, rf processing

1.0 INTRODUCTION

During the last decade, a series of high frequency rf breakdown experiments have been conducted at Stanford Linear Accelerator Center. This research has included accelerator structures[1,8], high power klystrons[2], microwave components[3], and single cavity X-band transmission cavities operating in the TM_{010}[4] and TM_{020} mode[3,5,6]. This paper will focus on the current experimental rf breakdown research utilizing the TM_{020} cavity. This cavity was developed as a relatively low cost structure in that the main body of the cavity and coupling waveguides can be repeatedly used from one experiment to the next. The high gradient section of the cavity is removable and is the only replacement part required. Initially, this cavity was tested inside an X-band travelling wave resonant ring. In this platform, microparticle contamination, dark current, grain boundaries, and surface plasma were investigated. A summary of this work is discussed, and the reader is referred to ref. [3,6] for a more detailed account of these experiments. RF Breakdown experiments are currently being conducted inside an X-band "windowtron". The windowtron isolates the TM_{020} cavity vacuum from the rf source (50-MW klystron) by two TE_{11} ceramic windows. This platform is being utilized to characterize and study the behavior of rf breakdown and dark current at pulse lengths ranging from 80ns to 1500ns. This platform is also being utilized to investigate rf breakdown in various vacuum conditions ranging from 10^{-11} to 10^{-5} Torr.

2.0 EXPERIMENTAL SETUP

The TM_{020} cavity (Fig. 1) has two removable copper noses designed to facilitate nondestructive analysis of the high gradient surface area. The mechanical joint between the fixed and removable section of the cavity is positioned at the peak of the second radial field maximum. This is a minimum rf current position reducing the possibility of arcing at the joint. The first radial field maximum for the TM_{020} mode is located at the center which has the appearance of a button (diameter of 0.5 cm) in the photograph. Viewports in-line with the cavity permit imaging of the high field surface areas. X-rays from field emitted electrons are monitored by a scintillator mounted outside the test structure. The scintillator is fiber optically coupled to a photomultiplier tube. After each experiment the cavity noses are removed and analyzed by a scanning electron microscope with energy dispersive x-ray analysis (SEM/EDX).

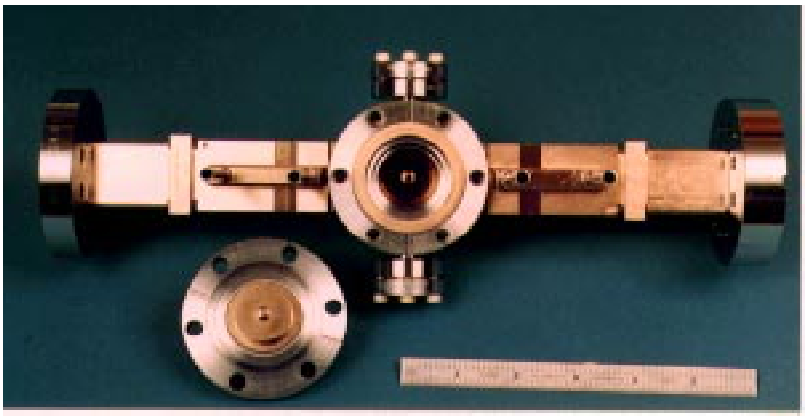

Figure 1. TM_{020} cavity with removable cavity nose shown in foreground. The length of the cavity and waveguide structure shown is approximately 12-inches.

Two platforms have been used in this research. Initially, the cavity was inserted into an X-band traveling wave resonant ring (TWR) shown schematically in Fig. 2a. The resonant ring gain is nominally 10-dB and is capable of providing up to 300 MW to trigger breakdown in the cavity. The resonant ring input source is a 30 MW X-band klystron designed to operate at 11.424 GHz. A fraction of the klystron power is coupled into the ring each rf cycle. The wave circulates around the ring and at the completion of each revolution the wave in-phase with the incident power results in wave reinforcement and power multiplication. In this platform, microparticle contamination, dark current, grain boundaries, and surface plasma have been investigated.

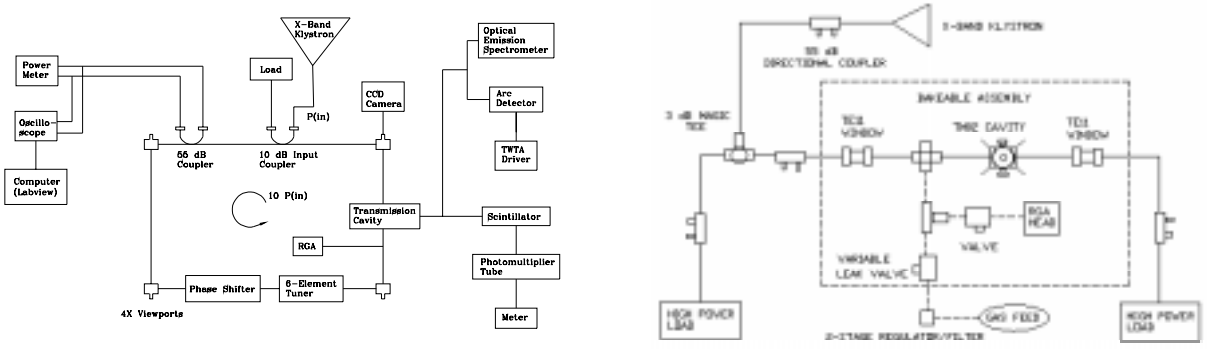

(a) (b)

Figure 2. Experimental setup for rf breakdown studies using a (a) traveling wave resonant ring and (b) a windowtron.

The second rf breakdown platform utilized in this research incorporates a windowtron. The windowtron isolates the rf breakdown test cavity vacuum from the rf source and load by two TE_{11} ceramic windows (Fig. 2b). This platform is designed to characterize the breakdown field and dark current as a function of pulse duration and in various vacuum conditions. The windowtron input source is a 50 MW X-band klystron operating at 11.424 GHz. The output power is first coupled into a 3-dB magic tee to protect the klystron from reflected power during a breakdown event in the cavity. The TE_{11} windows enable the cavity and components within the windowtron to be baked out as a complete assembly prior to rf testing. After bakeout, initial pressures of 10^{-11} Torr have been achieved. To measure rf breakdown at various vacuum levels, a variable leak valve is used to slowly introduce gas into the system. The background pressure in the cavity is monitored using an ultra-high

vacuum ionivac gauge (extractor gauge) that will read down to 10^{-12} Torr. The extractor gauge is mounted on the cavity perpendicular to the cavity noses. RF power is measured at the input and output of the cavity by two 55-dB directional couplers. A visible light arc detector is utilized to capture intrapulse breakdown events and is connected to a cavity viewport.

3.0 EXPERIMENTAL RESULTS

3.1 Summary of Travelling Wave Resonant Ring Results

In the first experiment, microparticles on the surface of the cavity noses were carefully tracked before and after rf processing. The results of this investigation showed that small particles (0.5-5μm) did not contribute significantly to rf breakdown. Particles of this size are what one may expect to find using good cleaning and handling techniques, without the benefit of a costly cleanroom facility. Experiments were also conducted with and without vacuum firing the demountable cavity noses. Breakdown sites were observed to follow grain boundaries for the cavity noses that were not vacuum fired (Fig. 3a). This experiment was repeated with a new set of cavity noses yielding the same results (Fig. 3b). This phenomenon occurs well below the limiting breakdown field, and is presumed to be caused by trapped gas at the grain boundaries that is liberated by surface heating during rf processing. Motivated by these findings a set of cavity noses were vacuum fired at 800°C for 24 hours. These cavity noses did not have the preferential breakdown sites along grain boundaries.

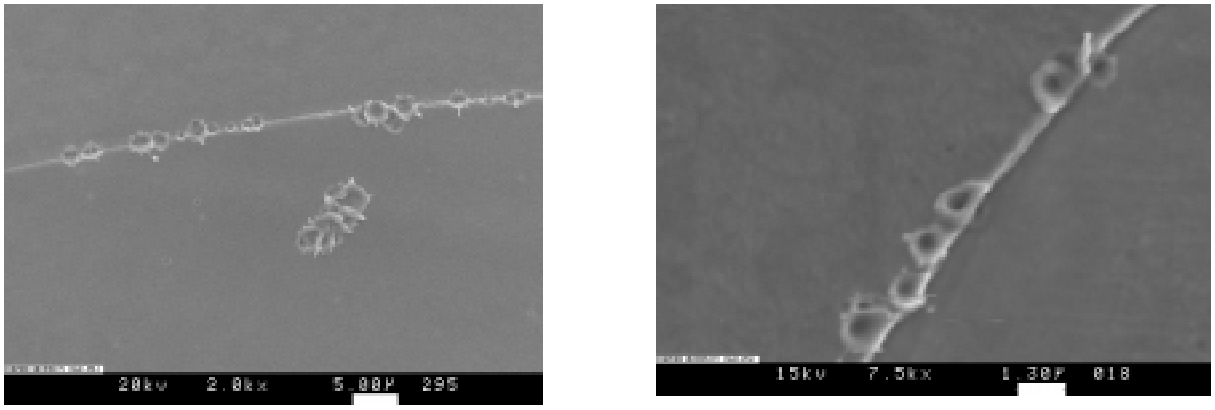

(a) (b)

Figure 3. SEM shows preferential breakdown along grain boundaries at field levels of ~150 MV/m for a rf pulse duration of 1.5 μs for the cavity noses that were not vacuum fired. (a) 1st experiment. (b) 2nd experiment.

Irreversible damage was observed to occur when the cavity was processed above the breakdown limit. This resulted in a significant increase in x-ray intensity for a given field strength, and a substantial decrease in the maximum attainable field level. When the breakdown field is not exceeded, the dark current measurements are repeatable for a conditioned surface. During a breakdown event, it appears that arcing occurs near the high field surface, but not across the gap (Fig. 4b). The first photograph in Fig. $4b_1$ shows a direct image of the high field surface area as observed by a CCD camera with an external light source. A drawing of how the cavity noses are situated in the cavity is provided in Fig. 4a. The ring in the background of this drawing gives a perspective of the viewing area as seen through the viewport. The remaining pictures in Fig. $4b_{2\text{-}4}$ are consecutive images taken in the breakdown region, where each frame represents one rf pulse (1.5μs). The two outside small images of light in Fig $4b_{3\text{-}4}$ are reflections from the arcs on the waveguide walls.

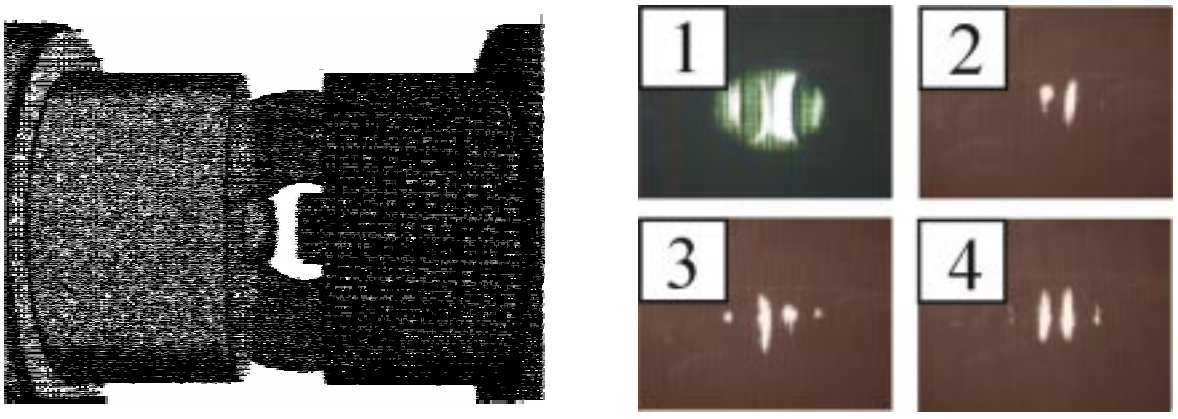

(a) (b)

Fig. 4. (a) Drawing of the cavity noses situated inside the cavity. The gap distance between the noses is 0.075 inches. The ring in the background gives a perspective of the viewing area as seen through the viewport. (b_1) Image of high field surface area with external light source. (b_2) emission site on left and reflection on right side. (b_3) Emission site on right and reflection on left side. (b_4) Emission and reflection on both sides.

The two inside light images are of primary interest. It is believed that the smaller circular spot is due to the emission site, while the crescent image is reflection from the cavity nose due to the opposing (circular image) emission site. This crescent effect is also noticeable in Fig. 4.b_1 from the external light source.

3.2 Windowtron Data And Results

Recent experiments have investigated vacuum conditions and pulse duration and their relationship to rf breakdown. This section will begin with the pulse length experimental study. In the experiments discussed in the previous section, pulse length variations were limited by the high loaded Q and subsequently the long fill time (500ns) of the resonant ring. In the windowtron design the fill time of the cavity is ~75ns, enabling a study of breakdown field behavior at pulse lengths ranging between 80ns-1500ns.

3.2.1 Narrow rf pulse processing

Two sets of copper cavity noses were rf processed at a pulse length of 150ns. The first set of cavity noses was installed into the windowtron and the structure was baked out at 450^{o}C for three days prior to rf testing. After bakeout, the pressure measured by the extractor gauge at the cavity was $5x10^{-11}$ and varied up to $4x10^{-10}$ during rf processing. During rf processing, the power was gradually increased until a field gradient of 500 MV/m was measured across the gap. In this test, the cavity noses were removed and examined prior to achieving the maximum attainable field. The cavity noses were SEM analyzed to examine the topography of the surface (Fig. 5a). At 50 times magnification, rf breakdown sites were evident and significant deformation of the surface was observed.

A second set of OFE copper cavity noses were tested and removed after processing to a field gradient of 350 MV/m. In this experiment, the cavity noses were vacuum fired and the windowtron structure was heat tape baked at 150^{o}C for three days. The initial vacuum was measured at $6x10^{-10}$ Torr. This is approximately an order of magnitude lower in vacuum than the previous experiment where the entire assembly was baked out at 450^{o}C. The pressure varied between $2x10^{-10}$ and $1x10^{-9}$ Torr during rf processing. The surface of the cavity nose showed only a few breakdown sites (Fig. 5b) and no signs of thermal stress or fatigue was noticeable.

It is clear that surface heating is occurring somewhere between 350-500 MV/m for an rf pulse length of 150ns. For the TM_{020} mode, the azimuthal magnetic field increases with an increase in the radial distance. In Fig. 5a, the deformation of the surface decreases as a function of radial distance, and therefore is probably not due to electromagnetic energy. The surface stress may be caused by field emitted electron bombardment of the surface.

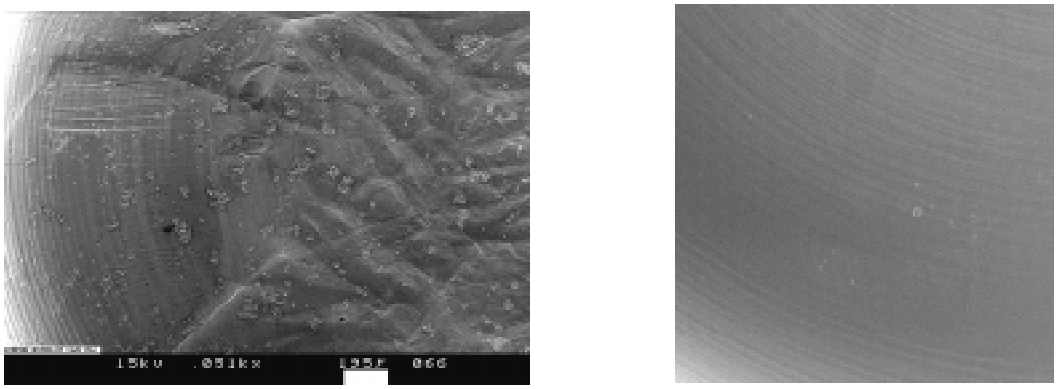

(a) (b)

Figure 5. SEM photograph showing one quadrant of the cavity nose surface area after rf processing at field levels of (a) 500 MV/m (50X) and (b) 350 MV/m (75X). Surface heating is occurring between 350MV/m-500MV/m.

3.2.2 80ns-1500ns rf pulse processing

Breakdown fields depend on pulse length (at narrow pulse lengths), and closely approach CW breakdown fields ($dE/d\tau \approx 0$) for sufficiently long pulses. This section investigates the pulse length (τ^{-n}) dependence of breakdown fields in the nonlinear region ranging from 80ns to 1500ns.

In this experiment, the cavity was initially processed at the shortest possible pulse length (80ns) and the breakdown field was measured versus pulse length up to 1500ns. The experimental data (solid line) is given in Fig. 6 and is compared to a normalized field following a $\tau_p^{-1/3}$ and $\tau_p^{-1/2}$ time behavior. For pulse lengths between 800-1500ns, the breakdown field followed a $\tau^{-1/2}$ dependence, which one might expect when considering average power (P_{avg}),

$$E \propto \frac{K\sqrt{P_{avg}}}{\tau_p^{\frac{1}{2}}}, \tag{1}$$

where K is a constant related to cavity geometry and pulse repetition rate, and τ_p is the pulse duration. At shorter pulse durations a transition (600ns-800ns) in the breakdown field from $\tau^{-1/2}$ to $\tau^{-1/3}$ occurs. The physical mechanism that lowers the breakdown field time behavior from $\tau^{-1/2}$ to $\tau^{-1/3}$ at pulse lengths less than 800ns is currently being investigated. In a second experiment, the transition occurred between 800ns-1000ns. In both experiments, thermal stress and fatigue on the surface were apparent.

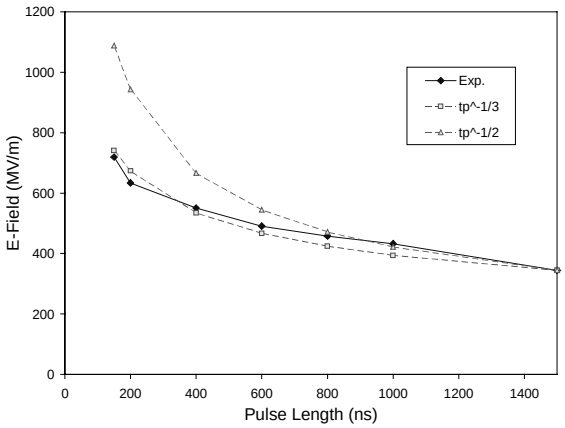

Figure 6. Breakdown field at various pulse lengths. The measured experimental (Exp.) field gradient is compared to a normalized field following a $t_p^{-1/3}$ and $t_p^{-1/2}$ time behavior.

Field emission occurs when very high electric fields are applied to a metallic surface. The Fowler-Nordheim (FN) equation[7] can be used to calculate the field emission current density and for rf fields is given by[8]:

$$J_{FN} = \frac{5.7x10^{-12}\, x10^{4.52\phi^{-0.5}}\, (\beta Eo)^{2.5}}{\phi^{1.75}} \exp\frac{-6.53x10^{9}\, x\phi^{1.5}}{\beta Eo}, \qquad (2)$$

where ϕ is the work function (4.5eV for copper), Eo is the peak electric field, and β is a field enhancement factor due to protrusions, contamination, oxide layers, dielectric inclusions, grain boundaries, or adsorbates. Field emission in rf structures is generally detected one to two orders of magnitude lower than predicted by the FN equation without the correction factor, β. When field emitted electrons are accelerated across the gap and collide with the opposing cavity nose, bremsstrahlung x-rays are produced by the sudden retardation of the electrons. These x-rays are monitored by a scintillator that is fiber optically coupled to a photomultiplier tube. By correlating the x-rays to the dark current, and by using the FN equation (Eqn. 2), the field enhancement factor, β, is determined. In these experiments, β ranged typically from 25-35 up to field levels of 250MV/m (Fig. 7a). Above 250 MV/m, the current density is limited by the Child-Langmuir law for space charge limited current (J_{CL}). In this region, the current continues to increase but at a much slower rate then predicted by the FN equation. The calculated field emission current density (J_{FE}) for various β's are plotted in Fig. 7b, along with the space charge limited current density (J_{CL}) for a gap distance of 2mm. For a β of 19, the intersection between J_{CL} and J_{FN} occurs at 250 MV/m. This corresponds to the experimental data (Fig. 7a), where a decrease in current is observed beginning at approximately 250 MV/m (plotted as $1/E*10^{-9}$). The combination of the calculated J_{FN} and J_{CL} current density is plotted in Fig. 8a. When taking into account the space charge limited current, the calculated FN graph (Fig. 8b) closely approximates the experimental data (Fig. 7a). Measuring dark currently indirectly, does not take into account that the scintillator output may increase with x-ray energy. This would suggest a lower field enhancement factor than measured (Fig. 7a). Calibration experiments are currently being designed to determine the scintillator energy dependence.

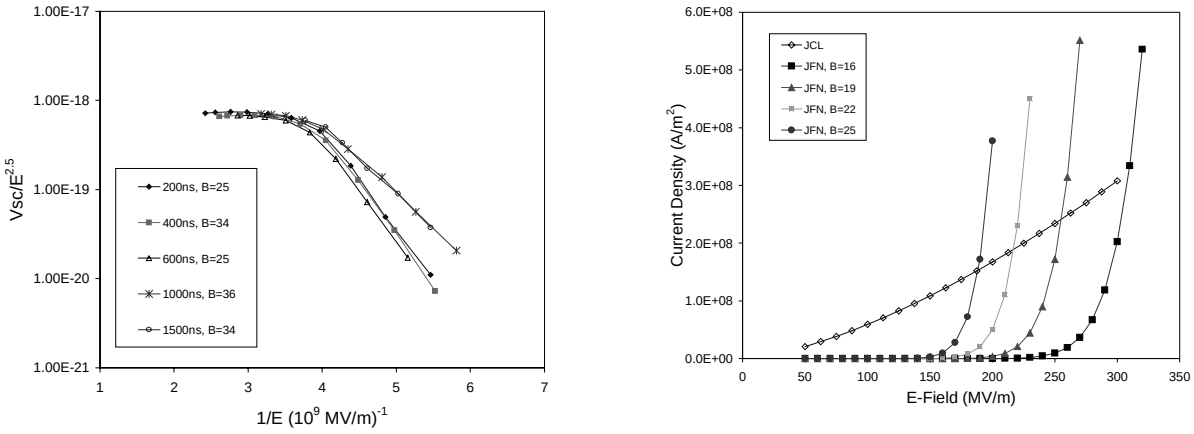

(a) (b)

Figure 7. Fowler-Nordheim plot showing the field enhancement factor to be ~25-35 in the linear region (log scale). At 250MV/m, the current decreases. (Vsc is the x-ray intensity measured by a scintillator). (b) Calculated field emission current density for various β's. Also shown is the Child Langmuir space charge limited current for a gap distance of 2 mm.

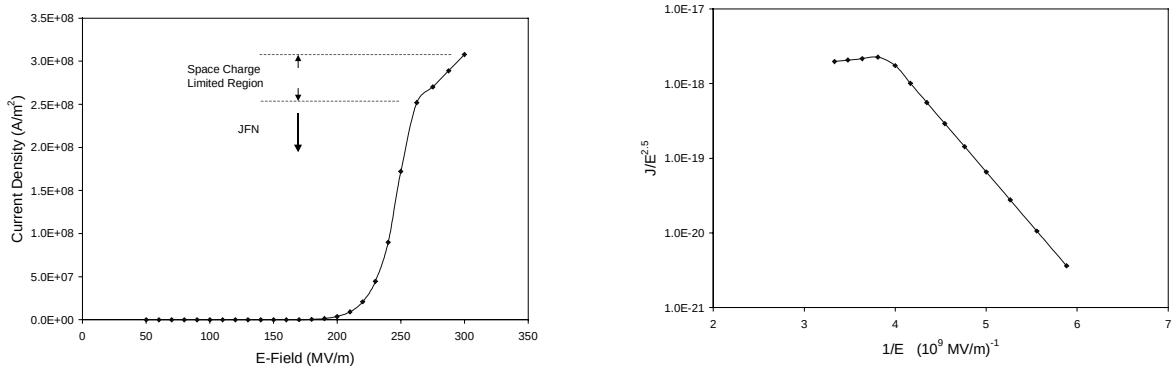

(a) (b)

Figure 8. Plot of calculated field emission current density for a β of 19 with space charge effects included. (b) Fowler-Nordheim plot of Fig. 8a with space charge limited current included resembles experimental data (Fig. 7a).

3.2.3 Vacuum variations

The importance of ultrahigh vacuum relative to medium/high vacuum is under investigation. Although this study is preliminary in scope, the experimental results have been unexpected. This section compares the breakdown fields and dark current at pressures ranging from 10^{-11} to 10^{-5} Torr. In this study, the cavity is first rf processed at the best attainable vacuum. Gas is then systematically introduced into the system while monitoring dark current and breakdown. In Fig. 4, a surface plasma was detected near the cavity nose during breakdown. By increasing the background pressure in the cavity, one would expect an increase in fragmentation and ionization probability, and subsequently a lower breakdown field. Two experiments have been conducted to investigate the importance of vacuum conditions and to determine if a breakdown relationship exists in the medium to ultrahigh vacuum range.

3.2.3.1 RF processing at various pressures with nitrogen

For the first variable background pressure experiment, nitrogen gas was selected primarily due to convenience and availability. Prior to testing, the windowtron was baked for two weeks at 450°C. After installation into the rf system a starting vacuum of $5x10^{-11}$ Torr was measured at the cavity. The initial step was to determine the change in dark current as a function of pressure while maintaining the field strength below breakdown fields. The gas is fed through a two-stage regulator and filtered prior to introducing the gas into the windowtron. The pressure was varied from 10^{-11} to 10^{-6} Torr. At each pressure, the pulse length was incremented in 200ns steps over the interval of 200-1000ns. For a constant gradient of 250 MV/m, the dark current remained approximately the same throughout five orders of magnitude in pressure (Fig. 9a). The gas was pumped out of the system and the constant gradient constraint was removed. The dark current was again measured at various pressures up to field strengths sufficient to initiate breakdown. To minimize surface damage, two pulse lengths (200ns, 600ns) were tested. The highest attainable vacuum after pumping out the nitrogen gas followed by a heat tape bake for three days, was 10^{-10} Torr. For a pulse duration of 200ns, the onset of breakdown was 350 MV/m at 10^{-10} Torr (Fig. 9b). The pressure was increased to 10^{-8} Torr and the dark current measurements for a given field strength were approximately the same as the measurements taken at 10^{-10} Torr. There was an increase in field strength; however, this is believed to be due to the additional conditioning time. When the pressure was increased to 10^{-5} Torr, a small deviation in dark current is noticeable. A further increase in pressure is currently not available in this design. Nitrogen exists as a diatomic triple bond molecule, and has one of the strongest bonds found in any molecule. Nitrogen's lack of chemical reactivity is why it is regularly used in vacuum systems. The high ionization energy and lack of chemical reactivity may have been why no significant change in dark current was detected. This experiment was also conducted at a pulse duration of 600ns. The onset of breakdown was slightly lower and the dark current measurements at 600ns matched those taken at 200ns.

Afterwards, the cavity noses were removed and SEM/EDX analyzed. The result of rf processing with nitrogen appeared to cause an in-situ "plasma cleaning" with sufficient energy to cause surface ablation. Numerous small (< 2μm) copper particles were detected on the surface. The dark current did not increase substantially even with the additional "microparticles". This is consistent with the particle study discussed earlier.

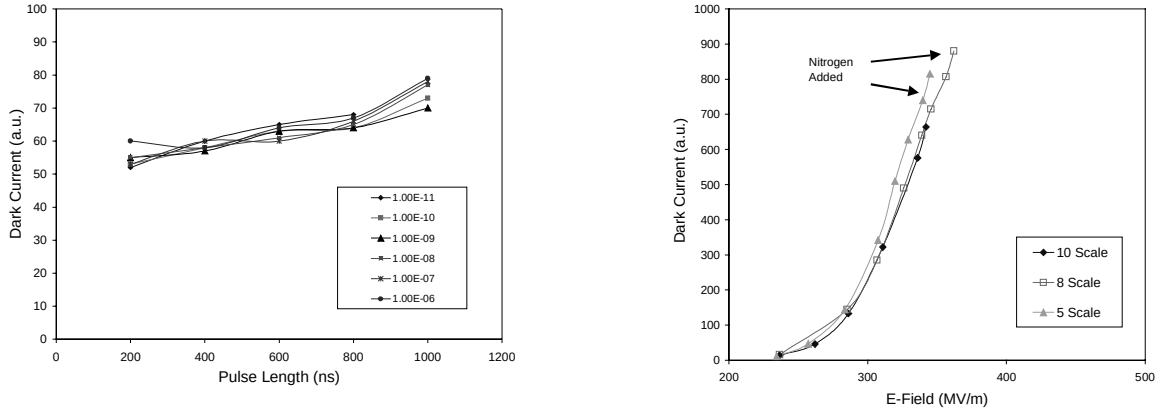

(a) (b)

Figure 9. RF processing with Nitrogen. (a) At field levels below breakdown fields (E=250 MV/m), dark current as measured by x-ray intensity, is approximately the same. (b) Dark current remained approximately the same while rf processing up to the onset of breakdown while background pressures ranged over five orders of magnitude (Pulse length is 200 ns).

3.2.3.2 RF processing at various pressures with CO_2

CO, CO_2, and hydrogen, are gases that are typically observed in ultrahigh vacuum systems, and research studies[9,10] have suggested that carbon particles are more likely to become field emitters compared to other elements or compounds. For these reasons, a carbon-based gas (CO_2) was selected and tested at various pressures up to the onset of breakdown.

In this experiment a new set of cavity noses were vacuum fired at 800°C prior to rf testing. The windowtron structure was heat tape baked at 150°C. The starting pressure inside the cavity was 10^{-9} Torr. Dark current measurements as a function of field strength are given in Fig. 10. In Step 1, the dark current was measured prior to introducing CO_2 into the system and a field gradient of 450 MV/m was achieved. In Step 2, CO_2 was introduced incrementally at pressures ranging from 10^{-7} to 10^{-5} Torr. The dark current increased by almost a factor of two compared to the measurements without CO_2. After the initial CO_2 was introduced at 10^{-7} Torr, the dark current did not continue to increase as a function of gas density between 10^{-7} and 10^{-5} Torr. The onset of breakdown (end point) was the same with and without CO_2 in the system (~410 MV/m). In Step 3, the gas was pumped out of the cavity bringing the pressure back down to 10^{-9} Torr. The magnitude of the dark current closely followed the dark current measurements taken prior to introducing gas into the system (Step 1). Note that the onset of breakdown is higher and is believed due to additional conditioning time. In Step 4, the cavity was rf processed for a period of 60 hours and the dark current decreased by approximately a factor of two compared to those taken without CO_2 in the system. The roll off in dark current at higher field levels is due to scintillator saturation.

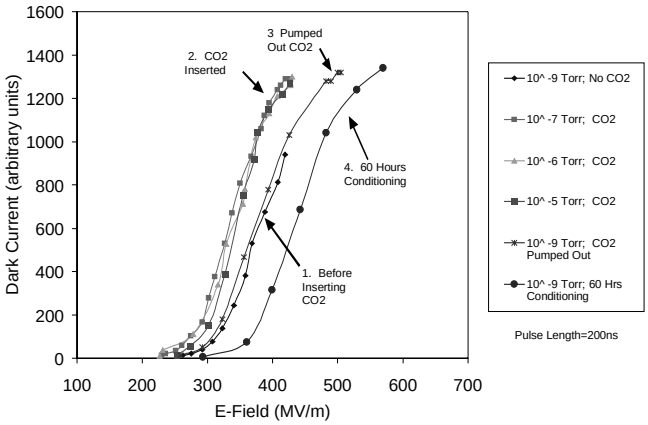

Figure 10. Introducing controlled amounts of CO_2 into the cavity increased the dark current; however, the onset of breakdown remained the same. After pumping the CO_2 out of the system, the dark current followed the curve taken prior to introducing the gas. The lowest dark current was observed after conditioning for 60 hours. (Pulse length is 200 ns)

3.2.4 Effects of short term atmosphere exposure

In the field of high power microwaves, it is necessary at times to expose components and/or microwave sources to atmosphere for modifications or repairs. The question arises as to what effect breaking vacuum will have on a surface that has already been processed. In this experiment, the cavity was rf processed for several weeks until the maximum attainable field gradient was achieved. Afterwards, the cavity noses were removed from vacuum. This process included a nitrogen purge, minimal atmospheric exposure, and a 30-hour detainment in a nitrogen filled hot box. After the cavity noses were inserted back into the cavity, the windowtron was heat tape baked for 72 hours. In this experiment, power levels up to 80% of those previously acquired were quickly achieved. Processing through the remaining 20% was comparable in time to processing an unconditioned surface.

4.0 FUTURE AREAS OF STUDY

In the output cavity of the 50 MW X-band klystrons, rf breakdown has been observed to occur predominantly on the iris's facing the collector. This may suggest that x-ray radiation, due to beam bombardment in the collector, may be connected to the breakdown process. Experiments are currently being designed to determine if x-rays are a trigger mechanism in the breakdown process. This will be accomplished by directing x-rays generated from the collector of a nearby klystron at the rf breakdown cavity. A key feature of this setup is the ability to vary the x-ray energy and intensity by controlling the beam voltage and power.

RF processing high power microwave sources and components can be time consuming and costly. During processing, a reduction in field emission is observed suggesting that emission sites can be removed and/or their geometry modified. Although, it is still unclear if there is a relationship between dark current and breakdown, there are applications (i.e. accelerators) that are adversely affected by the presence of dark current. Two common types of rf processing are standard rf processing and high peak power narrow pulse processing. Standard rf conditioning refers to rf processing with progressively higher power levels at the designed pulse length. High peak power narrow pulse processing limits the amount of available energy in breakdown events that occur while processing. This method initially processes at reduced pulse lengths in order to melt potentially explosive emission sites that may cause surface damage at wider pulses. A comparison between these two processing methods will emphasize time, dark current, and breakdown threshold.

Future experiments will include comparing the effects of surface finish, and materials on the rf breakdown threshold. Typical surface roughness for the copper cavity noses has ranged from 8-12 μ-inches. Three sets of single-point-diamond turned cavity noses have been fabricated and are ready for testing. The results of this test will be compared to standard machining. Materials (Cu-W, Glidcop) that may be less susceptible to thermal stress will also be tested.

5.0 CONCLUSIONS

RF processing with nitrogen and CO_2 at various pressures show that dark current appears to be gas specie dependent. When nitrogen was introduced into the cavity, the dark current and breakdown field was nominally affected. When CO_2 was injected, the dark current increased by a factor of two; however, the onset of breakdown occurred at the same field strength as compared to ultrahigh vacuum (10^{-11} Torr). This indicates that dark current is not directly related to breakdown. A correlation between breakdown field and pressures ranging from 10^{-11} to 10^{-5} Torr could not be resolved.

At field levels below 250MV/m, the dark current followed the Fowler-Nordheim equation (J_{FN}) for β's of 25-35. Above 250 MV/m, the dark current was observed to decrease substantially. The field-emitted current density is probably limited in this region by the Child-Langmuir law for space charge limited current (J_{CL}). This was found to be consistent with the theoretical calculations for current density. These calculations included space charge effects for a gap distance of 2-mm and a β of 19.

This study has also investigated the pulse length (τ^{-n}) dependence of breakdown fields for pulse durations ranging from 80n to 1500ns. Between 800ns to 1500ns, the breakdown fields were observed to follow a $\tau^{-1/2}$ time behavior. This might be expected when considering average power for pulse lengths less than the energy threshold where the field time behavior approaches CW. At shorter pulse durations (< 800ns), a transition in the breakdown field time behavior is evident, shifting from $\tau^{-1/2}$ to $\tau^{-1/3}$. This transition occurs above the space charge limited region where the field emission current continues to rise but at a much slower rate. The breakdown field at shorter pulse lengths occurs at field levels where there appears to be significant surface heating. The physical mechanism that reduces the breakdown field may be due, at least in part, to thermal mechanisms, although the source remains unclear.

ACKNOWLEDGEMENTS

The authors wish to express appreciation and acknowledge the efforts of the employees in the klystron department at SLAC. This work has been supported by the AFOSR under Grant F49620-95-1-0253 (MURI), and by the Department of Energy contract DE-AC03-76SF00515

REFERENCES

1. G.A. Loew, J.W. Wang, "RF Breakdown Studies in Room Temperature Electron Linac Structures", SLAC-PUB-4647, May 1988.
2. A.E. Vlieks, et al., "Breakdown Phenomena in High Power Klystrons", SLAC-PUB-4546, March 1988.
3. L. Laurent, G. Scheitrum, A. Vlieks, C. Pearson, G. Caryotakis, N.C. Luhmann Jr, "RF Breakdown Experiments at SLAC", High Energy Density Microwaves (RF 98), Pajaro Dunes, CA, pp. 261-278.
4. X. Xu, R. Callin, W. Fowkes, et al, "RF Breakdown Studies in X-band Klystron Cavities", SLAC-PUB-7505, May, 1997.

5. L. Laurent, G. Scheitrum, et al., “High Gradient RF Breakdown Study”, presented at the Microwave Vacuum Electron Device Conference, Monterey, CA, May 1998.
6. H. Krompholz, L. Laurent, Y. Lau, A. Neuber, “Windows and rf Breakdown”, Advances in High Power Microwave Sources and Technologies, R. Barker, E. Schamiloglu, editor, IEEE Press, To be published Nov. 2000.
7. R.H. Fowler, L.W. Nordheim, “Electron Emission in Intense Electric fields”, Proc. Royal Soc., vol. 119A, p. 173, 1928.
8. J.W. Wang, “RF Properties of Periodic Accelerating Structures for Linear Colliders”, SLAC-Report 339, pg. 105, July 1989.
9. P. Niedermann, “Experiments on Enhanced Field Emission”, PhD Thesis, University of Geneva, 1986.
10. J. Knobloch, “Advanced Thermometry Studies of Superconducting RF Cavities”, PhD Thesis, Cornell University, 1997.